Journal of Atmospheric and Terrestrial Physics, Vol. 56, No. 2, pp. 209–221, 1994
Printed in Great Britain

Pergamon Press Ltd

Polar cap potential distributions during periods of positive IMF B_y and B_z

WILLIAM J. BURKE,* EWA M. BASINSKA,† NELSON C. MAYNARD,*
WILLIAM B. HANSON,‡ JAMES A. SLAVIN§ and J. DAVID WINNINGHAM‖

*Geophysics Directorate, PL/GPSG, Hanscom AFB, MA 01731, U.S.A.; †Boston University, Center for Space Physics, Boston, MA 02215, U.S.A.; ‡University of Texas at Dallas, Richardson, TX 75080, U.S.A.; §NASA Goddard Space Flight Center, Greenbelt, MD 20771, U.S.A.; ‖Southwest Research Institute, San Antonio, TX 78284, U.S.A.

(*Received in final form* 26 *March* 1992; *accepted* 27 *March* 1992)

Abstract—We compare the DE-2 electric field measurements used by HEPPNER and MAYNARD [(1987) *J. geophys. Res.* **92**, 4467] to illustrate strongly distorted, BC convection patterns for IMF $B_z > 0$ and large $|B_y|$, with simultaneous detections of particle spectra, plasma drifts and magnetic perturbations. Measured potentials (>50 keV) driven by the solar wind speeds exceeding 500 km/s, are greater than published correlation analysis predictions by up to 27%. The potential distributions show only two extrema and thus support the basic conclusion that under these conditions the solar wind IMF drives two- rather than four-cell convection patterns. However, several aspects of the distorted two-cell convection pattern must be revised. In addition to the strong east–west convection in the vicinity of the cusp, indicated by Heppner and Maynard, we also detect comparable components of sunward (equatorward) plasma flow. Combined equipotential and particle precipitation distributions indicate the presence of a lobe cell embedded within the larger, afternoon reconnection cell. Both types rotate in the same sense, with the lobe cell carrying 20–40% of the total afternoon cell potential. We detected no lobe cell within morning convection cell.

INTRODUCTION

Because of their strong correlations with the levels of geomagnetic activity at auroral latitudes, much attention has been given to cases in which the interplanetary magnetic field (IMF) has a southward, negative Z, component. A southward IMF drives antisunward convection across the polar cap with return flow through the auroral zone (HEPPNER, 1972). The Y component of the IMF affects the distribution plasma convection, equivalently electric potential, within the polar cap. In the northern hemisphere, with positive IMF B_y, convection tends to be stronger on the dawn flank of the polar cap. Negative IMF B_y produces strong convection along the dusk flank of the polar cap. In the southern hemisphere the opposite convention applies. Situations with strong convection along the dawn and dusk flanks of the polar cap are referred to as BC and DE convection patterns, respectively, by HEPPNER and MAYNARD (1987).

RUSSELL (1972) extended the model of DUNGEY (1961) to include northward IMF. The revised model postulates that merging occurs between the IMF and open field lines at the magnetopause, abutting the poleward boundary of the dayside cusp. It consequently predicts the development of sunward convection within the polar cap. Measurements by MALZAWA (1976) confirmed this prediction. During periods of northward IMF, magnetic perturbations at the ground indicated the presence of two convection cells in the polar cap with polarities opposite to those with southward IMF. Electric fields detected by BURKE *et al.* (1979) near the dawn–dusk meridian showed four convection cells, with sunward flows in the auroral oval and central polar cap and with antisunward flows along the flanks of the polar cap. They suggested that auroral convection cells were driven by plasma flows in the low-latitude boundary layer [LLBL] (EASTMAN *et al.*, 1976). Electric field measurements by the DE-2 satellite, from a wider range of local times, indicated that northward IMF convection patterns are rotations and distortions of normal, two-cell patterns (HEPPNER and MAYNARD, 1987).

The reversed polarity two-cell (MALZAWA, 1976) and the four-cell (BURKE *et al.*, 1979) convection patterns are easily reconciled, and henceforth we only refer to the four-cell pattern. They are, however difficult to reconcile with the distorted two-cell patterns of HEPPNER and MAYNARD (1987). A review of the two- vs four-cell convection pattern controversy is given by BURKE (1988). Recently KNIPP *et al.* (1991) using the Assimilative Mapping of Ionospheric Electrodynamics [AMIE] procedure (RICHMOND and KAMIDE, 1988), and MCCORMAC *et al.* (1991) using measured neutral wind dynamics, suggested that the

large-scale convection pattern depends on the ratio IMF $|B_y|/B_z$. Both types of patterns develop during periods of northward IMF. When $|B_y|/B_z < 1$ the convection pattern has two distorted cells. If IMF B_z is the dominant component, four cells exist with two reversed-flow cells in the polar cap.

This paper seeks to increase our understanding of high-latitude phenomenology during periods when IMF $B_z > 0$ and $|B_y|$ is large. HEPPNER and MAYNARD (1987) showed two levels of rotation and existing of the two-cell pattern labeled weakly and strongly distorted. We have re-examined the potential distributions measured during the DE-2 orbits used to illustrate the strongly distorted BC convection pattern, reproduced here as Fig. 1. This convection pattern is found in the northern hemisphere when IMF $B_y > 0$ and in the southern hemisphere when IMF $B_y < 0$. Under these conditions magnetic tension effects produce strong, antisunward flows along the dawn flank of the polar cap. During periods of northward IMF the centers of the BC pattern cells rotate toward earlier local times. In the strongly distorted case, flow lines are sunward in the central polar cap, then twist toward the antisunward direction along the dusk flank of the cap.

The convection patterns of HEPPNER and MAYNARD (1987) were derived, using pattern-recognition techniques, from DE-2 north–south electric field measurements and their resulting potential distributions along the satellite trajectory. To the degree possible we have combined measured electric field and potential distributions with simultaneous detections of energetic ion/electron fluxes, plasma drifts and magnetic-field perturbations perpendicular to the Earth's main field. The two components of the electric field or plasma drifts and magnetic perturbations perpendicular to the magnetic field provide guidance for constructing large-scale convection patterns by indicating the directions of equipotential lines at their intersections with DE-2 trajectories. This paper extends the work of MAYNARD *et al.* (1991) and BASINSKA *et al.* (1992) who have investigated the ionospheric signatures of magnetic merging at the magnetopause under southward and northward IMF conditions, respectively.

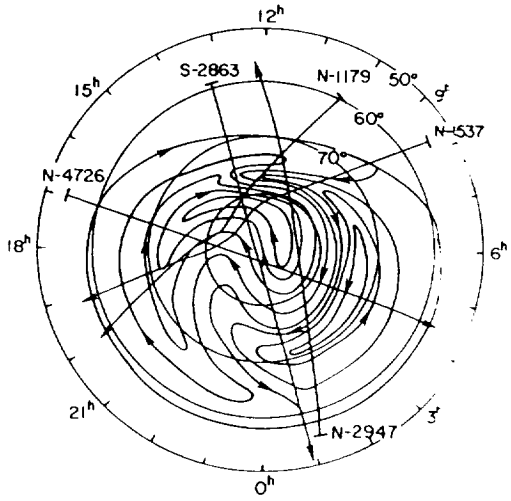

Fig. 1. The strongly distorted BC convection pattern of HEPPNER and MAYNARD (1987) with DE-2 trajectories used in this analysis superposed. Equipotentials/streamlines are plotted on a magnetic latitude (MLAT) vs magnetic local time (MLT) grid.

We also take advantage of the recent efforts to understand the interactions of the dayside magnetosphere–ionosphere system (cf. review by CROOKER and BURKE, 1991). Of particular relevance is a series of papers by the Johns Hopkins Applied Physics Laboratory group analyzing sources of particle precipitation (NEWELL and MENG, 1988; NEWELL *et al.* 1991a, b) and magnetic perturbations (BYTHROW *et al.*, 1988; ERLANDSON *et al.*, 1988), detected at ionospheric altitudes. Dayside precipitation source-regions include the cusp, the plasma mantle, the low-latitude boundary layer [LLBL], the boundary plasma sheet [BPS] and the central plasma sheet [CPS] (NEWELL *et al.*, 1991b). Because particles come from sources both inside and outside the magnetosphere, their detection provides qualitative information about the topologies of magnetic fields traversed by the satellite.

The following section gives a brief description of the DE-2's instrumentation package. Data acquired during five orbits of DE-2 are presented and the large-scale potential/convection patterns estimated. In the discussion section we compare these potential distributions with the Heppner–Maynard distorted BC pattern. Measured high-latitude potentials were quite large, in all cases exceeding 50 kV. Their distributions show two extrema and are thus consistent with a distorted, two-cell convection pattern. However, simultaneously measured particle fluxes indicate that the afternoon convection cell consists of a lobe cell embedded in a larger reconnection cell, both having the same sense of rotation. A convection model of REIFF and BURCH (1985) contains a lobe cell embedded in a reconnection cell with the same sense of rotation as presented here. It was attributed to conditions with IMF $B_y > 0$, but B_z directed southward.

INSTRUMENTATION AND MEASUREMENTS

DE-2 was launched into a 90° inclination, polar orbit on 3 August 1981. The satellite was three-axis

stabilized. A special issue of *Space Science Instrumentation* contains detailed descriptions of the Dynamics Explorer missions and instrumentation. Data examined in this paper come from the vector electric field instrument [VEFI] (Maynard *et al.*, 1981), the low-altitude plasma instrument [LAPI] (Winningham *et al.*, 1981), the vector magnetometer [MAG-B] (Farthing *et al.*, 1981), and the retarding potential analyzer [RPA] (Hanson *et al.*, 1981).

The VEFI used a double floating probe to measure DC and AC electric fields. The instrument consisted of two cylindrical dipoles to measure the two components of electric field in the spin plane of the spacecraft. Its primary purpose was to monitor the convective electric fields and the intensities of low frequency waves at auroral and polar-cap latitudes. In this paper we use the DC measurements to deduce the potential distribution along the satellite trajectory and the component of plasma drift normal to the magnetic field and the satellite trajectory. The component of plasma drift along the trajectory was calculated from the RPA measurements.

MAG-B was a triaxial fluxgate magnetometer placed at the end of a 6 m astromast boom. Sensor outputs were sampled sixteen times per second with a digital resolution of ± 1.5 nT. The major factor limiting the absolute accuracy of the vector magnetic field comes from uncertainties regarding the spacecraft/boom attitude, which may be several tenths of a degree. The stability of DE-2 during any given pass is such that measurements of field-aligned currents densities are accurate to better than 0.1 $\mu A/m^2$.

The LAPI experiment provided measurements of both positive ion and electron fluxes from 5 eV to 32 keV in 32 energy bins, at 15 different pitch angles, each sampled once every second. The instrument was designed so that the same energy bins were sampled simultaneously at the different pitch angles. LAPI also contained Geiger–Mueller (G–M) counters to detect fluxes of electrons with energies > 35 keV. They are mounted on a scan platform and measure fluxes at pitch angles of 0 and 90.

Figure 1 represents the strongly distorted BC convection cell with five superposed DE-2 trajectories in magnetic latitude (MLAT) and magnetic local time (MLT). Four of the orbits were used in fig. 13 of Heppner and Maynard (1987) to illustrate how this pattern was derived. All orbits were chosen from periods when the IMF had a nearly constant orientation for several hours, and thus should drive steady convection patterns. We have added a fifth orbit, No. 2947 from 17 February 1982, which came at the end of a long period of northward IMF. The cusp portion of orbit No. 2947 has been studied in detail by Basinska *et al.* (1992). Different levels of satellite data coverage are available from the five orbits. Electric and magnetic field measurements were taken in all cases. LAPI measurements were retrieved during all orbits except No. 4726. RPA measurements of the along-trajectory component of plasma drift were only taken during orbits No. 1179, 2863 and 2947. The hourly averaged values of solar wind IMF parameters at the times of the passes are listed for reference in Table 1. Note that during all of these orbits, solar wind speeds > 500 km/s were measured.

In Fig. 1 the distorted BC convection pattern is characterized by two large-scale convection cells. The afternoon and morning cells are approximately centered at 12 MLT, 82° MLAT and at 05 MLT, 73° MLAT, respectively. On the dayside, at the statistical location of the cusp, near 12 MLT and 80° MLAT (Newell and Meng, 1988), convection is almost purely east–west with a small antisunward component. At subcusp latitudes near magnetic noon, equipotentials are quite contorted, with significant overlap between the morning and afternoon cells. The strongest antisunward flows are located along the dawn flank of the polar cap. In the central polar cap, plasma flows sunward, then diverts to move antisunward along the dusk flank of the polar cap before returning to sunward flow in the afternoon or morning sectors of the auroral oval.

Figures 2 and 3 illustrate the complex of measurements forming the basis of the present analysis. Figure 2 contains 15 min of VEFI and LAPI measurements taken at northern high latitudes during DE-2 orbit No. 1179. The pass traverses the late morning and early evening MLT sectors. Electric field, plasma drift and magnetic field measurements are displayed in a satellite-centered coordinate system. The X and Y axes are positive along the direction of satellite motion and toward zenith, respectively. The Z axis completes the right-hand system. E_X in the top panel of Fig. 2, is small and varies smoothly except between 0644:30 and 0646:00 UT. The onset of E-field turbulence is marked by a poleward spike followed by an equatorward excursion (eastward convection) of ~ 30 s duration before turning poleward (westward convection). After 0647 UT the E-field was weak and predominantly negative in the satellite-centered system.

A data gap exists in particle measurements from 0643:30 to 0644:30 UT. Prior to this, both the Geiger Mueller tube [GMT] > 35 keV (second panel) and the lower energy electron (bottom panel) measurements indicate that the satellite crossed a region of plasma sheet precipitation. After the data gap the > 35 keV electron fluxes became isotropic, decreasing steadily to lower polar-cap levels of $\sim 5 \times 10^3$ e cm^{-2} s sr. In the

Table 1. Hour-averaged interplanetary parameters

Orbit	Date	UT	IMF (nT)			Solar wind	
			B_x	B_y	B_z	V (km s^{-1})	n (cm^{-3})
1179 N	22 October 1981	0650	2.2	12.9	5.0	519	14.2
1537 N	15 November 1981	0938	0.6	5.8	2.7	567	5.2
2863 S	12 February 1982	0520	0.5	15.6	18.6	528	2.7
2947 N	17 February 1982	0605	9.7	7.0	9.5	655	10.1
4726 N	15 June 1982	1025	2.2	4.6	3.1	561	8.3

2-min interval after data resumption we see relatively high fluxes of < 1 keV electrons and a V-shaped, energy-vs-time dispersion in the flux of precipitating ions. Ion dispersion shapes of this type are characteristic of the cusp during periods of northward IMF (Burch *et al.*, 1979). Poleward of the ion dispersion structure we find two discrete structures near 0647 and 0648 UT, with keV electron and ion precipitation. Between 0648:30 and 0653 UT the satellite detected polar rain interspersed with weakly accelerated electron structures. During the interval 0653–0656:30 UT, DE-2 encountered keV electron and ion fluxes characteristic of nightside boundary and central plasma sheet precipitation, respectively (Winningham *et al.*, 1975). Structured precipitation straddles the convection reversal boundary.

Figure 3 gives the electric potential distribution (top panel) obtained by integrating E_λ (second panel) along the satellite trajectory; the component of plamsa drift along the trajectory from the RPA (third panel), and the differences between the measured and MAGSAT model Z (fourth panel) and X (bottom panel) components of the magnetic field. The plot of E_λ is identical to that in Fig. 2 and is presented here for convenience in comparing data. The along-trajectory plasma drift is plotted as $-V_\lambda$, so that positive values are opposite to the direction of satellite motion. In the infinite current sheet approximation positive (negative) slope in the ΔB_z trace corresponds to field-aligned currents (FAC) into (out of) the ionosphere.

Several aspects of orbit No. 1179 N measurements deserve attention:

1. The potential is always negative indicating that only the afternoon convection cell was sampled. The location of the -55 kV potential minimum or convection reversal coincides with the boundary of cusp precipitation at the poleward edge of the ion dispersion structure.

2. From 0644 to 0648:20 UT the V_λ measurements indicate that convection had a sunward component. This interval spans the satellite crossing of the cusp and the two discrete electron and ion structures located poleward of the cusp. The maximum in $|V_\lambda|$ of 2 km/s at 0645:25 UT coincides with the maximum in E_λ which drives a westward component of plasma drift of ~ 3.5 km/s. V_λ was weakly sunward on the dayside of the polar cap and antisunward at night.

3. The variations in ΔB_z and ΔB_λ reasonably correlate with each other in the vicinity of the cusp and anticorrelate in the nightside auroral region. This indicates that the satellite crossed several extended, large-scale FAC sheets. The dayside currents flowed into the ionosphere near the equatorward part of cusp precipitation and outward in the poleward portion. The nightside currents had the polarities appropriate for the evening sector Region 1/Region 2 system (Iijima and Potemra, 1976).

Figure 4 combines plasma-drift and precipitating-particle measurements taken during DE-2 orbit No. 1179. The data are presented in the form of vector plasma drift measurements at 10 kV intervals along the satellite trajectory in an MLAT–MLT coordinate system. Equipotentials are then joined to each other consistent with their directions at their intersection with the satellite trajectory. The contours are drawn with no attempt at pattern synthesis away from the trajectory. In the afternoon/evening auroral oval the shape of equipotentials differs from the Heppner

Fig. 2. Electric field and particle measurements acquired during northern high-latitude portion of DE-2 orbit No. 1179 N plotted as functions of universal time (UT), satellite altitude (ALT), magnetic local time (MLT) and invariant latitude (IL). The top panel gives the component of the electric field along the direction of satellite motion E_λ. The second panel contains the flux of electrons with energies > 35 keV at pitch angles of 0° (yellow trace) and 90° (white trace). The bottom two panels are energy-vs-time color spectrograms of the energy flux from precipitating ions and electrons with energies between 5 eV and 32 keV.

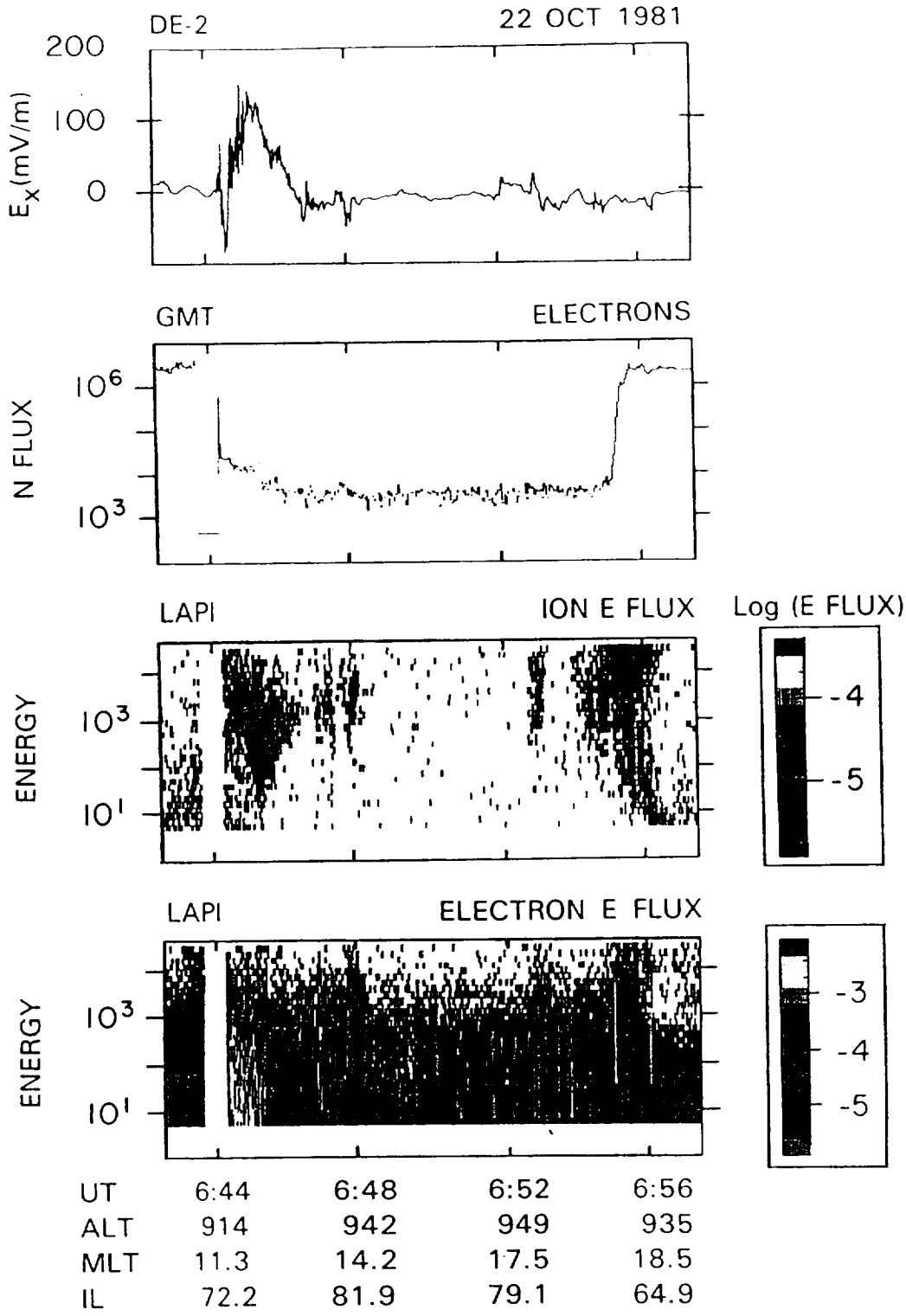
DE-2
22 OCT 1981
200
100
0
E_x(mV/m)
GMT
ELECTRONS
10^6
10^3
N FLUX
LAPI
ION E FLUX
Log (E FLUX)
10^3
10^1
ENERGY
-4
-5
LAPI
ELECTRON E FLUX
10^3
10^1
ENERGY
-3
-4
-5
UT 6:44 6:48 6:52 6:56
ALT 914 942 949 935
MLT 11.3 14.2 17.5 18.5
IL 72.2 81.9 79.1 64.9

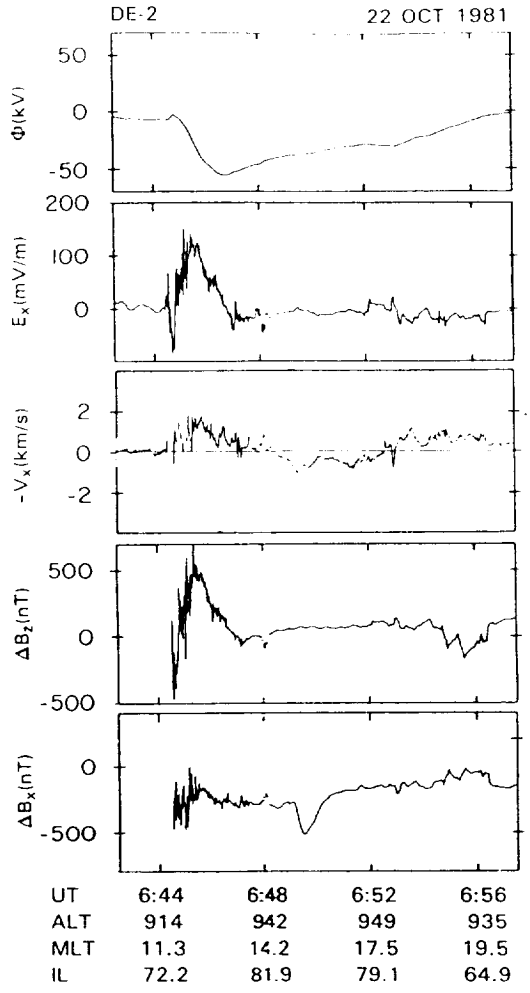

Fig. 3. The electric potential distribution (top panel) obtained by integrating E_x (second panel) along the satellite trajectory. The third panel contains the along-trajectory component of plasma flow—V_x, obtained from the RPA. The bottom two panels give the cross- (ΔB_Z) and along- (ΔB_X) trajectory perturbations of the Earth's magnetic field.

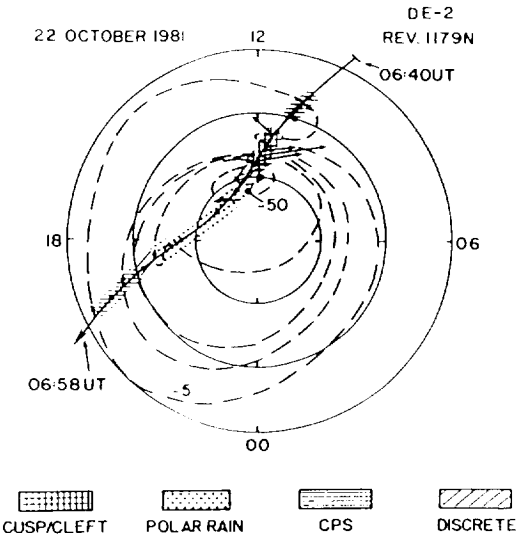

Fig. 4. The afternoon convection cell obtained by combining E_x and V_x measurements during DE-2 orbit No. 1179 N. The stream lines are at 10 kV intervals. Their directions at trajectory intersections are indicated by arrows. Away from the trajectories, representations are not unique. Particle fluxes are represented as cusp/cleft, polar rain, central plasma sheet and discrete precipitation.

Maynard pattern shown in Fig. 1. No information about the morning cell potential was retrieved during this pass. Note, however, that unlike the Heppner-Maynard pattern, ~20 kV out of the 55 kV total potential is contained in a small, clockwise rotating sub-cell within the polar cap. It is embedded in a larger, clockwise rotating convection cell whose flow lines close through the auroral oval.

The trajectory in Fig. 4 has been coded to indicate where various types of particle precipitation were encountered. For simplicity we divide the particle fluxes into four phenomenological categories:

(1) diffuse aurora, CPS precipitation (WINNINGHAM *et al.*, 1975),

(2) cusp/cleft precipitation (NEWELL and MENG, 1988),

(3) polar rain precipitation (WINNINGHAM and HEIKKILA, 1974), and

(4) discrete/structured precipitation.

The discrete/structured precipitation appears in the plasma mantle, the polar cap and auroral oval. It comes from diverse magnetospheric and magnetosheath sources.

Data retrieved during the remaining four orbits have been similarly analyzed and convection/precipitation patterns were derived. The results are summarized in Fig. 5. The potentials measured in the sampled portions of the afternoon and morning convection cells are listed in Table 2. In all five cases the potential distributions are consistent with at least part of the afternoon cell being confined to the polar cap. Although we sampled parts of the morning convection cell during all four orbits shown in Fig. 5, we found no evidence in the combined potential distribution and particle precipitation measurements indicating that a part of the morning cell was completely restricted to open field lines in the polar cap.

Since orbits No. 2863 and 2947 followed similar

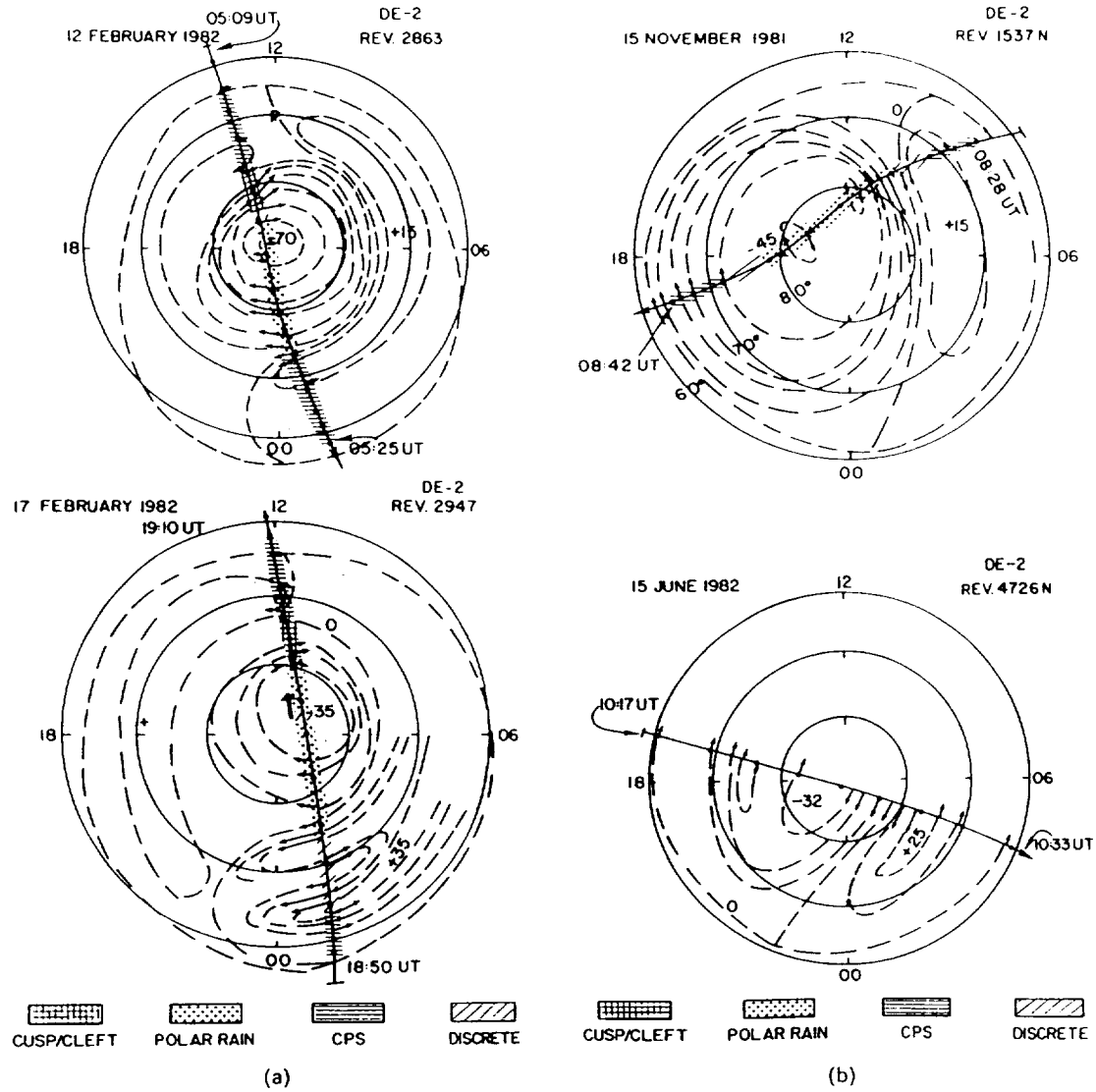

Fig. 5. Convection and particle precipitation patterns for (a) orbits 2863 and 2947, and (b) orbits 1537 and 4726, in the same format as Fig. 4.

Table 2. Trajectory and potential distributions

Orbit	MLT	Θ_{IMF}	Potential (kV)			
			Φ_{KL}	Φ_{pm}	Φ_{am}	Kp
1179 N	10.3–19.9	68.8	89	−55	—	4
1537 N	08.3–19.0	65.0	59	−50	20	4−
2863 S	13.3–00.5	40.0	69	−70	20	4−
2947 N	00.9–11.5	36.4	52	−35	36	2+
4726 N	16.9–04.5	56.0	50	−32	25	3−

trajectories it is useful to list points of similarity and dissimilarity in their measurements:

1. Orbits No. 2863 and 2947, like orbit No. 1179 (Fig. 4) passed close to magnetic noon through a region of negative potential characteristic of an encounter with the afternoon convection cell only on the dayside. In the case of orbit No. 2947 plasma convection at MLAT >80 on the dayside was almost purely sunward right up to the onset of cusp precipitation (BASINSKA *et al.*, 1992).

2. LAPI detected cusp cleft electron precipitation during both passes. Within most of this region, convection had sunward and westward components. As in orbit No. 1179, convection had an eastward component near the low-latitude boundary of cusp/cleft precipitation.

3. During orbit No. 2947 precipitating ions had an inverted dispersion (BURCH *et al.*, 1979) with the most energetic ions precipitating near the poleward boundary of the cusp and less energetic ions at lower latitudes. The precipitating ion flux during orbit No. 2863 was weak and had the energy-vs-latitude dispersion characteristic of $B_Z < 0$ IMF.

4. Poleward of the cusp precipitation, discrete ion and electron structures were detected during orbit No. 2863 but not No. 2947.

5. The large-scale, dayside FAC systems near local noon had morphologies similar to those of orbit No. 1179 (Fig. 3).

6. On the nightside, the convection and FAC patterns were somewhat distorted during orbit No. 2947. Within the auroral oval the BPL/CPS precipitation and Region 1/Region 2 FACs were typical of the morning convection cell for orbits No. 2863 and 2947.

During orbit No. 1537, DE-2 crossed the noon meridian at higher than cusp latitudes. In both the evening and dayside portions of the pass, discrete electron-precipitation structures straddled the convection reversal line. Within the dayside region of structured precipitation, ions had several keV of energy where convection was sunward and a few hundred eV where it was antisunward. In this latter region particles had characteristics of boundary plasma layer and plasma mantle rather than LLBL precipitation (NEWELL *et al.*, 1991a, b). The magnetic perturbations indicate the presence of FACs out of the ionosphere in the region of CPS and mantle precipitation and into the ionosphere in the region of BPL precipitation. Within the polar cap there is a broad region of stagnant plasma. Here MAYNARD *et al.* (1990) found an ionospheric-density depletion which met their criteria for the existence of a small cell completely contained within the polar cap.

DISCUSSION

In the previous section we presented the results of our analysis of five DE-2 orbits, four of which were used to illustrate the strongly distorted, BC convection cell of HEPPNER and MAYNARD (1987). Such convection patterns occur during periods of $B_Z > 0$, in the northern hemisphere when IMF $B_Y > 0$ and in the southern hemisphere when IMF $B_Y > 0$. First we compare the potential distributions of Figs 4 and 5 with that of HEPPNER and MAYNARD (1987) shown in Fig. 1. We then compare the magnitudes of the measured, high-latitude potentials with previously reported polar cap potential dependencies on the solar wind/IMF conditions. Finally, we combine the plasma-drift and precipitating particle flux measurements to suggest a phenomenological interpretation of the high-latitude convection pattern with $B_Z > 0$, a large B_Y component and high solar wind speeds.

Figure 1 shows that the strongly distorted BC convection pattern consists of two cells. The afternoon and morning cells are rotated having their minimum and maximum potentials centered at 12 MLT, 82° MLAT and 05 MLT, 80° MLAT, respectively. Near noon near the statistical location of the dayside cusp (NEWELL and MENG, 1988) plasma flows nearly westward with a small antisunward tilt. Poleward of the cusp, plasma initially flows antisunward along the dawn flank of the polar cap, then turns sunward into the central polar cap. Afternoon cell stream lines then twist toward the antisunward direction along the dusk flank of the cap before entering the auroral oval and return to the dayside. Positive potential stream lines of the morning cell are similarly contorted. Eventually they end up in the post-midnight portion of the auroral oval and then return to the dayside.

Adopting the pattern-recognition spirit of HEPPNER and MAYNARD (1987), and recognizing the dangers of deriving a pattern from only five passes, we have constructed a convection pattern that reproduces the main features found in the individual DE-2 passes. We anticipate that this interim pattern may be further refined when results from the study of a broader data set are incorporated. The synthesized convection pattern shown in Fig. 6 consists of two large cells whose centers are rotated away from the dawn–dusk meridian. In this pattern, we placed the equatorward boundary of the convection system at the statistical, equatorward boundary of auroral electron precipitation for $Kp = 3$ (HARDY *et al.*, 1981). We interpret this boundary as the ionospheric projection of the Alfvén shielding layer.

During DE-2 orbits No. 1179, 2863 and 2947 VEFI detected contorted, equipotential structures at sub-

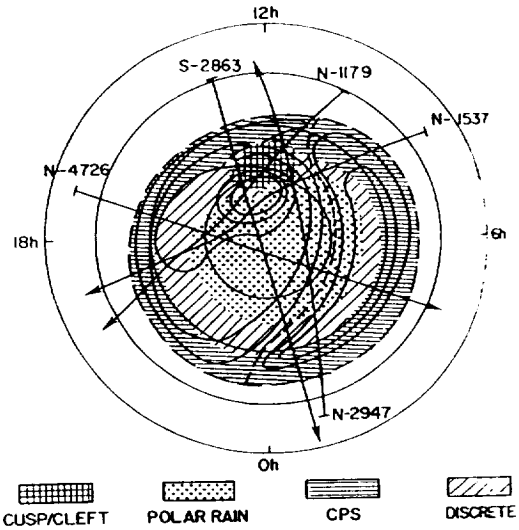

Fig. 6. Distorted BC convection/equipotential pattern representing the E_Y and V_Y data set obtained during the five DE-2 orbits.

cusp latitudes on the dayside. Unlike the Heppner–Maynard pattern shown in Fig. 1, the distortion is confined to the afternoon cell. Within the cusp, convection has both sunward and westward components. Equipotential contours of the afternoon cell can be divided into inner and outer regions. The innermost stream lines or equipotentials are confined to a small region in which LAPI detected cusp, polar rain and structured precipitation poleward of the cusp. Particles precipitating in these regions have sources in the magnetosheath. We assume that the magnetic field lines associated with these particle fluxes were always open. Thus, the equipotentials of this inner region reflect a circulation of magnetic flux within the northern lobe of the magnetotail and are referred to as a lobe cell (REIFF and BURCH, 1985). Up to 25 kV of the total polar cap potential was measured within the lobe cell. The remaining portion of the afternoon cell was encountered in regions of cusp, polar rain and auroral oval precipitation. Magnetic field lines along which such particle fluxes access the ionosphere are both open and closed. Plasma in the outer portion of the afternoon cell flows antisunward across the polar cap and returns to the dayside through the auroral oval. The morning cell contains no lobe cell, being made up of flow lines that pass through precipitation regions associated with both open and closed field lines. Magnetic field lines in convection cells with open and closed topologies circulate through the lobes of the magnetotail into the distant neutral sheet where they reconnect with field lines from the conjugate hemisphere. After reconnection, newly closed field lines convect in the earthward through the plasma sheet and equatorward in the auroral ionosphere. The group of equipotentials/streamlines containing both open and closed field lines are called reconnection cells by REIFF and BURCH (1985). We note in passing that, with the exception of the subcusp distortions, the reconnection portion of the afternoon cell in Fig. 6 closely resembles the weakly distorted BC pattern shown in fig. 11 of HEPPNER and MAYNARD (1987).

It is widely believed that during extended periods of northward IMF, geomagnetic activity decreases to very low levels. Information contained in Table 2 indicates that such was not the case at the times of our selected DE-2 orbits. The *Kp* index was between 2+ and 4, and the combined potentials sampled in the afternoon ($\Phi_{p.m.}$) and morning ($\Phi_{a.m.}$) cells ranged between 57 and 90 kV. The DE-2 trajectories across the inferred potential distributions of Figs 4 and 5 indicate that on any given pass, only a fraction of the total potential was sampled. Thus, the potentials listed in Table 2 only represent lower bounds on the actual, total cross-polar cap potentials.

Polar cap potential measurements from the OGO-6 (HEPPNER, 1972) Atmosphere Explorer (REIFF *et al.*, 1981), S3-2 (DOYLE and BURKE, 1983) and S3-3 (WYGANT *et al.*, 1983) satellites have been correlated with geomagnetic indices and solar wind/IMF parameters. Within the limits of small-sample statistics, these studies produced similar results. When comparing S3-2 measurements of the polar cap potential with hourly averaged solar wind/IMF parameters, DOYLE and BURKE (1983) found that the highest overall correlation coefficient came from the relationship:

$$\Phi_{KL}(\text{kV}) = 33.4 + 0.024\ E_{KL} \qquad (1)$$

where E_{KL} is the electric field function in the solar wind suggested by KAN and LEE (1979).

$$E_{KL} = V_{SW} B_T \sin^2(\Theta/2) \qquad (2)$$

where $B_T = [B_Y^2 + B_Z^2]^{1/2}$ and Θ are the magnitude and polar angle of the IMF when projected onto the GSM Y–Z plane. In calculating E_{KL} in equation (2) the solar wind speed is in km/s and the IMF components in nT. Table 2 lists the values of Θ and the statistically predicted values of Φ_{KL} which are between 89 and 50 kV. In all but one case, orbit No. 1179, these are less, by 13–27%, than the measured potentials.

The greatest discrepancy between the measured potential and the statistical-model predictions occurred on orbit No. 1179 where the measured potential is substantially smaller than the model pre-

diction. This is probably a sampling artifact. To increase the chances of representing the full high-latitude potential, the statistical models were derived from measurements taken by satellites in dawn–dusk orbits. During orbit No. 1179, DE-2 moved along a noon–midnight trajectory where it only encountered the afternoon cell. Presumably, the addition of potential from the morning cell at the time of this orbit would bring closer agreement with the statistical models. In the other four cases the statistical relationship in equation (1) also underestimated the total potentials contained in the afternoon and morning cells. The potential distributions in Figs 4 and 5 indicate that several tens of kV of the polar cap potential may be confined to small regions poleward of the cusp on the dayside of the polar cap. Satellite passes crossing the polar cap along the dawn–dusk meridian could miss a significant fraction of the lobe cell contribution to the total potential.

The convection/potential distribution in Fig. 6 summarizing the DE-2 measurements resembles the qualitative pattern found in fig. 7(f) of REIFF and BURCH (1985). It contains an afternoon reconnection cell surrounding a lobe cell that circulates with the same clockwise sense of rotation. The morning cell rotates counter-clockwise. However, their pattern was predicted for conditions with IMF $B_Y < 0$ and B_Z southward, *not* northward. In the representation of REIFF and BURCH (1985) viscous-driven cells are embedded in both the morning and afternoon cells. We noted that in the early evening sector the structured electron precipitation spanned the convection reversal region. It is possible that the antisunward part of this precipitation originates in the LLBL, analogous to the viscous cell of REIFF and BURCH (1985). It appears that cells tied to LLBL processes do not contribute significantly to the total high-latitude potential. Measurements by SMIDDY *et al.* (1980) show that the potential drop across the LLBL is typically < 10 kV.

The fact that a lobe circulation cell is embedded within the afternoon, negative potential cell, affects our understanding of the magnetosphere's interaction with the solar wind and a northward IMF. REIFF and BURCH (1985) suggested that during periods of large IMF B_Y both open and closed field lines present themselves to the solar wind on the dayside magnetopause. The IMF merges with Earth-bound field lines of both topologies. CROOKER (1988) proposed that with IMF $B_Y > B_Z > 0$, antiparallel merging is favored along lines located poleward of the cusp. They extend toward the dusk side of the cusp in the northern hemisphere and toward the dawn side of the cusp in the southern hemisphere.

Data presented above are consistent with merging occurring in both hemispheres. In the northern hemisphere the afternoon convection cell is driven by merging along a line extending toward dusk. It includes initially open field lines for the lobe cell and initially closed field lines for the reconnection cell. The morning cell is driven by merging along a line extending from a location poleward of the southern cusp toward dawn. Although merging occurs on both initially open and closed field lines, only initially closed lines of the reconnection cell are observable at northern latitudes. Figure 7(g) of REIFF and BURCH (1985) suggests that the converse may be true for southern hemisphere convection, where a distorted DE pattern (HEPPNER and MAYNARD, 1987) should appear.

Our interpretation differs from the model in fig. 6 of CROOKER (1988) which, for IMF $B_Y > B_Z > 0$ conditions, shows the ionospheric mapping of the merging line as a single V-shaped line on the afternoon side of the cusp. The model requires that both convection cells be driven from this merging line. As a consequence the morning cell wraps around the afternoon cell across local noon in such a way that a satellite passing close to the noon–midnight meridian must sample both convection cells. In the three cases where DE-2 passed through the cusp only the afternoon cell was sampled near noon. The model suggested by our measurements is merging driven for both cells and includes magnetic tension effects from IMF B_Y. It requires two merging lines in the ionosphere separated by a gap through which newly merged flux transports into the polar cap. In the northern hemisphere the merging line for the afternoon cell includes initially open and closed field lines. The morning cell in the northern ionosphere derives from the combined effects of viscosity as well as merging-driven, magnetic draping and tension processes in the southern hemisphere.

One intriguing aspect of our electric field data is the persistence of a latitudinally narrow strip of eastward convection near the equatorward boundary of cusp/cleft precipitation. Figure 2 shows that the eastward convection is located poleward of the onset of the electric field turbulence that marks the satellite entry into the cusp boundary (MAYNARD *et al.*, 1991). Here we develop two possible explanations consistent with the model described above. In both, initially closed field lines merge with the IMF at high latitudes on the dusk side of the cusp's magnetopause location. They differ only in the time scales required for magnetic tension to overcome stresses generated by local magnetosheath plasma flow (COWLEY *et al.*, 1983).

In the first hypothesis the magnetosheath-like particles originate on LLBL field lines whose equatorial footprints convect antisunward near the dusk mag-

netopause. At some point the near-cusp part of the field line merges and magnetic tension quickly causes the consequent westward motion. At latitudes of the eastward convection the soft particles propagate along the closed field lines of the LLBL; in places of westward convection they come directly from the magnetosheath on newly opened flux.

In the second explanation the soft particles come directly from the magnetosheath along open field lines in regions of both eastward and westward convection. This motion directly reflects the dynamics of dayside merging processes at locations away from the noon meridian. In the antiparallel merging scenario, this reflects merging with initially closed field lines somewhere poleward and to the afternoon of the cusp's location at the magnetopause. At merging sites located on the afternoon side of the cusp magnetosheath plasma flow has components that are antisunward and toward the dusk meridian. MAYNARD *et al.* (1991) have shown in a southward IMF B_Z case that the local plasma flow drags newly merged field lines in a direction opposite to that of magnetic tension. The magnetic stresses eventually win out. In the present cases with northward B_Z, the B_Y related magnetic stresses pull the field line toward the dawn meridian. However, because the IMF has a finite B_X and the draping topology is different from that for southward B_Z case, it takes longer for magnetic stresses to achieve dominance over the local, duskward magnetosheath flow, and cause field lines to eventually move in the westward direction (COWLEY *et al.*, 1983).

Acknowledgements—This work was supported by Air Force Office of Scientific Research Task 2311G5, by Air Force Contract No. F19628-90-K-0003 with Boston University, by NASA grants NAG-305 and NAG-306 with the University of Texas at Dallas and by NASA contracts NASW-4309 and NAGW-1621 with Southwest Research Institute.

REFERENCES

BASINSKA E. M., BURKE W. J., MAYNARD N. C., HUGHES W. J., WINNINGHAM J. D. and HANSON W. B.	1992	*J. geophys. Res.* **97**, 6369
BURCH J. L., FIELDS S. A. and HEELIS R. A.	1979	*J. geophys. Res.* **84**, 5863.
BURKE W. J.	1988	*Physics of Space Plasmas*, Vol. 8, p. 153. Scientific Publishers, Cambridge, Massachusetts.
BURKE W. J., KELLEY M. C., SAGALYN R. C., SMIDDY M. and LAI S. T.	1979	*Geophys. Res. Lett.* **6**, 21.
BYTHROW P. F., POTEMRA T. A., ERLANDSON R. E. and ZANETTI L. J.	1988	*J. geophys. Res.* **93**, 9804.
COWLEY S. W. H., SOUTHWOOD D. J. and SAUNDERS M. A.	1983	*Planet. Space Sci.* **31**, 1237.
CROOKER N. U.	1988	*J. geophys. Res.* **93**, 7338.
CROOKER N. U. and BURKE W. J.	1991	U.S. Nat. Rept 1987–1990, p. 1017.
DOYLE M. A. and BURKE W. J.	1983	*J. geophys. Res.* **88**, 9125.
DUNGEY J. W.	1961	*Phys. Rev. Lett.* **6**, 47.
EASTMAN T. E., HONES E. W. JR, BAME S. J. and ASBRIDGE J. R.	1976	*Geophys. Res. Lett.* **3**, 685.
ERLANDSON R. E., ZANETTI L. J., POTEMRA T. A., BYTHROW P. F. and LUNDIN R.	1988	*J. geophys. Res.* **93**, 9804.
FARTHING W. H., SUGIURA S., LEDLEY B. G. and CAHILL L. J. JR	1981	*Space Sci. Inst.* **5**, 551.
HANSON W. B., HEELIS R. A., POWER R. A., LIPPINCOTT C. R., ZUCCARO D. R., HOLT B. J., HARMON L. H. and SANATANI S.	1981	*Space Sci. Inst.* **5**, 503.
HARDY D. A., GUSSENHOVEN M. S., HOLMAN E., BURKE W. J. and HEINEMANN N.	1981	*J. geophys. Res.* **86**, 9961.
HEPPNER J. P.	1972	*J. geophys. Res.* **77**, 4877.
HEPPNER J. P. and MAYNARD N. C.	1987	*J. geophys. Res.* **92**, 4467.
HOFFMAN R. A. and SCHMERLING E. R.	1981	*Space Sci. Inst.* **5**, 345.
IIJIMA T. and POTEMRA T. A.	1976	*J. geophys. Res.* **81**, 2165.
KAN J. R. and BURKE W. J.	1985	*J. geophys. Res.* **90**, 4171.
KAN J. R. and LEE L. C.	1979	*Geophys. Res. Lett.* **6**, 577.
KNIPP D. J., RICHMOND A. D., EMERY B., CROOKER N. U., DE LA BEAUJARDIERE O., EVANS D. and KROEHL H.	1991	*Geophys. Res. Lett.* **18**, 721.
MAEZAWA K.	1976	*J. geophys. Res.* **81**, 2289.

MAYNARD N. C., AGGSON T. L., BASINSKA E. M., BURKE W. J., CRAVEN P., PETERSON W. K., SUGIURA M. and WEIMER D. R.	1991	*J. geophys. Res.* **96**, 3505.
MAYNARD N. C., BIELECKI E. A. and BURDICK H. F.	1981	*Space Sci. Inst.* **5**, 523.
MAYNARD N. C., SOJKA J. J., SCHUNK R. W., HEPPNER J. P. and BRACE L. H.	1990	*Planet. Space Sci.* **38**, 1077.
MCCORMAC F. G., KILLEEN T. L. and THAYER J. P.	1991	*J. geophys. Res.* **96**, 115.
NEWELL P. T., BURKE W. J., MENG C.-I., SANCHEZ E. R. and GREENSPAN M. E.	1991a	*J. geophys. Res.* **96**, 35.
NEWELL P. T., BURKE W. J., SANCHEZ E. R., MENG C.-I., GREENSPAN M. E. and CLAUER C. R.	1991b	*J. geophys. Res.* **96**, 21,013.
NEWELL P. T. and MENG C. I.	1988	*J. geophys. Res.* **93**, 14,549.
REIFF P. H. and BURCH J. L.	1985	*J. geophys. Res.* **90**, 1595.
REIFF P. H., SPIRO R. W. and HILL T. W.	1981	*J. geophys. Res.* **86**, 7639.
RICHMOND A. D. and KAMIDE Y.	1988	*J. geophys. Res.* **92**, 4467.
RUSSELL C. T.	1972	*Critical Problems of Magnetospheric Physics* (E. E. R. DYER ed.), p. 1. IUCSTP Nat. Acad. Sci., Washington, D.C.
SMIDDY M., BURKE W. J., KELLEY M. C., SAFLEKOS N. A., GUSSENHOVEN M. S., HARDY D. A. and RICH F. J.	1980	*J. geophys. Res.* **85**, 6811.
WINNINGHAM J. D., BURCH J. L., EAKER N., BLEVINS V. A. and HOFFMAN R. A.	1981	*Space Sci. Inst.* **5**, 465.
WINNINGHAM J. D. and HEIKKILA W. J.	1974	*J. geophys. Res.* **79**, 949.
WINNINGHAM J. D., YASUHARA F., AKASOFU S.-I. and HEIKKILA W. J.	1975	*J. geophys. Res.* **80**, 3148.
WYGANT J. R., TORBERT R. B. and MOZER F. S.	1983	*J. geophys. Res.* **88**, 5727.